OPEN

A Frequently Missed Pulmonary Infarction

Clinical and ^{18}F-FDG PET/CT Manifestation of Hilar Tumor–Induced Pulmonary Infarction

Yu Ji, MD, Yaru Wang, MD,* Chunchun Shao, MD,† Yong Cui, MD,* Na Su, BD,‡ Guangrui Shao, MD,* and Jingsong Zheng, MD‡*

Purpose: This study aimed to summarize the clinical and ^{18}F-FDG PET/CT manifestations of hilar tumor–induced pulmonary infarction.

Methods: A retrospective analysis was performed on patients with hilar masses who underwent FDG PET/CT scans between July 2015 and January 2021 and had complete clinical data. Pulmonary infarction was confirmed by concurrent chest CT and imaging follow-up or pathology.

Results: A total of 58 patients (mean age, 56 [SD, 13] years; 44 males) with 122 infarcts were included in the study. Hilar masses were mostly associated with small cell lung cancer (64%). The most common clinical manifestations were cough (64%) and hemoptysis (36%). Most patients (62%) had multiple pulmonary infarcts. The CT findings of pulmonary infarcts included the "Hampton hump" (48%) and patchy consolidation (52%). The density of infarcts included "bubbly consolidation" (61%) and "homogenous consolidation" (39%). The metabolic activity of 95 infarcts (78%) was higher than lung parenchyma, with the SUV_{max} of 3.3 (SD, 1.1). The metabolic patterns on PET/CT were "rim sign," "mismatch between PET and CT," and "no metabolism." Pulmonary vein involvement was found in 25 patients (43%), pleural effusion in 22 patients (38%), and the pleural curvilinear sign in 8 patients (14%).

Conclusions: The clinical manifestations of hilar tumor–induced pulmonary infarction are not specific, and ^{18}F-FDG PET/CT could be an effective diagnostic tool.

Key Words: ^{18}F-FDG, hilar tumor, PET/CT, pulmonary infarction

(*Clin Nucl Med* 2022;47: 473–479)

Pulmonary infarction refers to coagulation necrosis caused by a reduction in pulmonary perfusion.[1] Normal lung tissues receive a dual blood supply from the pulmonary arterial circulation and the bronchial arterial circulation. When the blood supply from the pulmonary arteries is insufficient, the bronchial arteries increase their blood perfusion to the ischemic area through physiological anastomosis between the two; thus, pulmonary infarction is infrequent.[2,3] However, if both arterial supply systems are blocked, the lack of reperfusion will lead to pulmonary infarction. Tsao et al[2] found in autopsy results that emboli with a diameter smaller than 3 mm in the distal pulmonary artery could significantly increase the incidence of pulmonary infarction. Kirchner et al[4] showed that the distance from an embolus in the pulmonary artery to the pleura is negatively correlated with the incidence of pulmonary infarction. These findings seem to indicate that obstruction of distal vessels is the leading cause of pulmonary infarction. However, in our clinical practice, we have found that the presence of a malignant mass at the hilum may also lead to pulmonary infarction. Such a mass involves only the hilar segment of the pulmonary artery and not the distal segment, and no sign of tumor emboli is evident in the distal lung tissue.[5] This type of pulmonary infarction is different from the common pulmonary infarction caused by emboli. We defined this type of infarction as hilar tumor–induced pulmonary infarction.

As ^{18}F-FDG PET/CT is widely used in diagnosis and evaluation of pulmonary tumors, it makes it necessary to accurately identify pulmonary infarcts on PET/CT images. Pulmonary infarction is accompanied by varying degrees of inflammatory responses, which will increase the utilization of glucose, leading to increased FDG uptake. Therefore, pulmonary infarction is easily confused with inflammation and tumors. An accurate understanding of the FDG PET/CT manifestations of pulmonary infarction can avoid antibiotic abuse, excessive tumor staging, unnecessary biopsy, and inappropriate treatment and improve the management of tumor patients.[6,7] However, only a few FDG PET/CT-related studies on pulmonary infarction are available, all of which are case reports or small cohort studies.[8,9]

This study aims to describe the clinical and FDG PET/CT manifestations of hilar tumor–induced pulmonary infarction through a comprehensive retrospective analysis of the clinical and imaging data of patients with this condition.

PATIENTS AND METHODS

This study was approved by our review boards for clinical investigations. All methods were performed in accordance with the Declaration of Helsinki and relevant guidelines. Because of the retrospective nature of the study, informed consent was waived.

Selection of PET/CT Images

We retrospectively analyzed 33,831 patients who underwent FDG PET/CT examination in 2 hospitals between July 2015 and January 2021. In our image archiving and retrieval system, we used the fuzzy keywords "hilar mass," "central lung cancer," "hilar tumor," and "hilar metastasis" in the first retrieval, and 3465 patients

Received for publication October 22, 2021; revision accepted February 10, 2022.
From the Departments of *Radiology and †Hospital-Acquired Infection Control, The Second Hospital, Cheeloo College of Medicine, Shandong University; and ‡Department of PET/CT, Shandong Cancer Hospital and Institute, Shandong First Medical University and Shandong Academy of Medical Sciences, Jinan, Shandong, China.
Author Contributions: JJ.Z. and Y.J. had full access to all of the data in the study and take responsibility for the integrity of the data and the accuracy of the data analysis, including especially any adverse effects. Y.J., N.S., and Y.W. contributed to the study design and data analysis and interpretation. Y.J., J.Z. and G.S. contributed to data analysis and interpretation. Y.J., Y.W., C.S., and Y.C. contributed to writing of the manuscript. JJ.Z. and G.S. contributed to critically revising of the manuscript.

Conflicts of interest and sources of funding: none declared.
Correspondence to: Jingsong Zheng, MD, Department of PET/CT, Shandong Cancer Hospital and Institute, Shandong First Medical University and Shandong Academy of Medical Sciences, 440 Jiyan Road, 250117, Jinan, Shandong, China. E-mail: 17660086108@163.com.

ISSN: 0363-9762/22/4706–0473
DOI: 10.1097/RLU.0000000000004180

remained after the first screening. The fuzzy keywords "pulmonary infarction" and "obstructive diseases" were used in the second retrieval, and 2032 patients remained. After manually excluding patients with no contrast-enhanced CT examination (within 3 days before or after FDG PET/CT examination) or with incomplete follow-up data after treatment, the remaining 169 patients were screened according to the diagnostic criteria for pulmonary infarction. Ultimately, 58 patients were included in the study.

Scan Technique

Imaging of patients was conducted on a PET/CT scanner (TF Big Bore [Philips, The Netherlands] and Ingenuity TF [Philips, The Netherlands]). ^{18}F-FDG with a pH of 5 to 7 and a radiochemical purity exceeding 95% were produced using a cyclotron (MINItrace; GE Healthcare, Milwaukee, Wis). The patients fasted for at least 6 hours and had blood glucose levels of less than 200 mg/dL prior to injection with ^{18}F-FDG. Patients lay in a quiet room 60 minutes after intravenous injection with 4.4 to 5.5 MBq/kg ^{18}F-FDG.

Spiral CT scanning was performed at 120 kVp and 300 mA · s. PET was performed after spiral CT without patient repositioning. PET images were obtained at 7 to 8 couch positions per patient, with an acquisition time of 1.5 minutes per position. We used CT scan data for attenuation correction of PET images and then fused the attenuation-corrected PET and CT images.

Chest contrast-enhanced CT examinations were performed using various helical scanners, as different hospitals and different CT scanners were involved in this study. All examinations were performed with 16- to 128-detector-row CT systems. CT acquisition parameters were 0.625- to 2.5-mm section thickness, 0.9 to 1.75 pitch, 120 kV, 80 to 350 mA · s, or automatic tube current adjustment. All examinations were performed with 50 to 100 mL of nonionic iso-osmolar contrast medium. Image reconstruction included contiguous 1- to 2-mm-thick sections with high resolution and standard algorithms for evaluation of the lung parenchyma and mediastinum. Patients were examined using the single-breath-hold technique. Analyses were performed on at least 2 reconstruction planes (usually axial and coronal reconstruction).

Reference Standard

The presence of infarction based on pathological biopsy or the following criteria (adapted from criteria suggested by Bray et al[10] and Revel et al[11]) was confirmed as follows:

(1) Manifestations on images:
   (a) An apparent mass at the hilum, occlusion, or obvious stenosis of the adjacent segment of the pulmonary artery present in at least 2 consecutive image sections and no filling or mild filling by the contrast agent in the distal segment of the pulmonary artery
   (b) Pulmonary parenchymal opacities in peripheral areas of the pulmonary arterial blood supply
   (c) No or only mild peripheral enhancement on contrast-enhanced CT images
   (d) Pulmonary opacity diminishing in size over time (melting sign) with complete resolution or leaving residual plate-like scarring and focal pleural thickening

(2) Patients with the following situations were excluded:
   (a) Changes in lung structures caused by any of a number of underlying diseases (lung fibrosis, severe emphysema, tuberculosis, interstitial lung diseases, etc) or surgery
   (b) Other lung diseases (obstructive pneumonia, atelectasis, etc) that may cause confusion in the diagnosis of pulmonary infarction
   (c) Laboratory test results (white blood cell count, neutrophil count, blood/sputum culture, etc) suggesting possible infectious lesions in the lungs

Reading Sessions

The images were reviewed by 3 readers (2 nuclear medicine physicians and 1 radiologist) blinded to the original study interpretation and report but with knowledge of the clinical tumor. All readers were asked to independently analyze the following imaging findings of all subjects: the number, morphology, density, metabolic level, and metabolic pattern of infarcts; pulmonary vein involvement; manifestations of affected pulmonary lobes; and pleural effusion. Differences in interpretations were resolved through consultation. If readers could not resolve discrepancies regarding the imaging results, the case was excluded.

TABLE 1. Participant Demographics

Parameter	Value
Sex, n (%)	
Male	44 (76)
Female	14 (24)
Age, y	
Range	21–81
Mean (SD)	56 (13)
Median	59
Tumor type, n (%)	
Small cell lung cancer	37 (64)
Adenocarcinoma	9 (16)
Cervical cancer	2 (3)
Squamous cell carcinoma	6 (10)
Sarcoma	2 (3)
Lymphoma	1 (2)
Adenosquamous carcinoma	1 (2)
Clinical feature, n (%)	
Cough	37 (64)
Hemoptysis	21 (36)
Dyspnea	9 (16)
Chest pain	8 (14)
Fever	7 (12)
No. infarcted lobes, n (%)	
Single	47 (81)
Multiple	11 (19)
Pulmonary vein involvement, n (%)	
Yes	23 (40)
No	30 (52)
Unable to determine	5 (8)
Pulmonary congestion, n (%)	
Yes	21 (36)
No	37 (64)
Pleural effusion, n (%)	
Yes	22 (38)
No	36 (62)
Pleural curvilinear sign, n (%)	
Yes	8 (14)
No	50 (86)

The data are the numbers of participants (n = 58) with percentages in parentheses, unless specified otherwise.

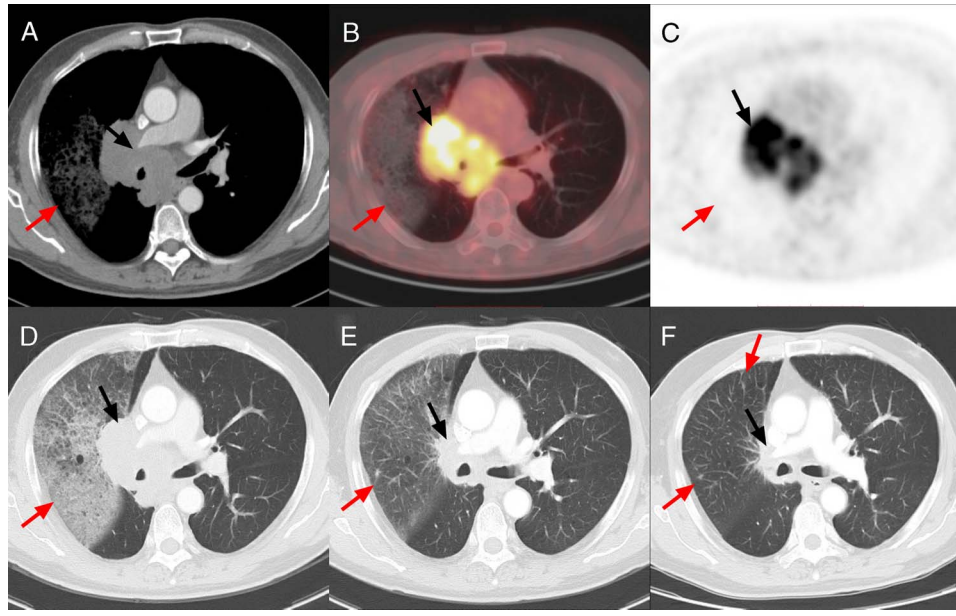

FIGURE 1. A 67-year-old man with small cell lung cancer of the right hilum. Axial contrast-enhanced CT (**A**), PET/CT (**B**), PET (**C**), and thin-slice chest CT (**D**) showed an FDG hypermetabolic mass (SUV_{max} = 11.2) in the right hilum (black arrow) with occlusion of the right pulmonary artery. A large pulmonary infarction was observed in the upper lobe of the right lung with no obvious FDG metabolism (red arrow). After 40 and 80 days of antitumor treatment, axial thin-slice chest CT (**E** and **F**) showed the mass in the right hilum was significantly reduced, and the right pulmonary artery was patent (black arrow). Pulmonary infarction diminished in size over time, leaving a residual fibrous scar (red arrow).

Follow-up

All patients received at least 1 FDG PET/CT or chest CT follow-up within 2 months after pulmonary infarction diagnosis. Because this study mainly investigated the FDG PET/CT manifestations of hilar tumor–induced pulmonary infarction, the main purpose of follow-up was to ensure the accuracy of the pulmonary infarction diagnosis.

Statistical Analysis

All data are expressed as the mean (SD). The clinical data and scan results of the patients were analyzed using descriptive statistics, including frequencies, means, and medians. All statistical analyses were performed in SPSS (version 23.0; IBM) for Microsoft Windows.

RESULTS

Demographic and Clinical Data

A total of 58 patients with hilar tumor–induced pulmonary infarction and complete data were included in the final study. Among the 58 cases of pulmonary infarction, 52 cases were confirmed by imaging, and 6 cases were pathologically confirmed. The 58 subjects were 21 to 81 years old (mean age, 56 [SD, 13] years), including 44 males and 14 females. The types of hilar tumors in these patients included primary tumors (10 cases: 6 cases of squamous cell carcinoma, 2 cases of sarcoma, 1 case of lymphoma, and 1 case of adenosquamous carcinoma) and hilar metastases (48 cases: 37 cases of small cell lung cancer, 9 cases of adenocarcinoma, and 2 cases of cervical cancer). The clinical manifestations were mainly cough and hemoptysis, followed by dyspnea, chest pain, and fever (Table 1).

CT Findings

A total of 122 pulmonary infarcts were found in our 58 patients. Sixteen patients had solitary infarcts, 18 had 2 infarcts, 10

TABLE 2. Pulmonary Infarction Characteristics

Parameter	Value
No. infarcted lesions	
1	16 (28)
2	18 (31)
3	10 (17)
4	6 (10)
5	2 (4)
Large infarct	6 (10)
Lobar location	
Left upper	40 (33)
Left lower	22 (18)
Right upper	38 (31)
Right middle	4 (3)
Right lower	18 (15)
CT findings	
Hampton hump	58 (48)
Patchy/nodular	64 (52)
Density	
Bubbly consolidation	74 (61)
Homogeneous consolidation	48 (39)
FDG metabolism	
Rim sign	42 (34)
Mismatch between PET and CT	53 (44)
No	27 (22)
SUV_{max}, range (mean [SD])	
Pulmonary infarcts	1.5–6.6 (3.3 [1.1])
Pleural curvilinear sign	2.4–5.0 (3.4 [0.8])

The data are numbers of infarcts (n = 122), with percentages in parentheses, unless specified otherwise.

had 3 infarcts, 6 had 4 infarcts, 2 had 5 infarcts, and 6 had multiple infarcts fused with each other, manifesting as a large diffuse infarct (with the range exceeding 1 lung segment) (Fig. 1). Forty infarcts were in the left upper lobe, 22 in the left lower lobe, 38 in the right upper lobe, 4 in the right middle lobe, and 18 in the right lower lobe. Forty-seven patients had single-lobe involvement, and 11 patients had ipsilateral multilobe involvement (Tables 1, 2).

Among the 122 infarcts, 58 manifested as a "Hampton hump" (48%), and the rest manifested as patchy or nodular consolidation (52%) (Fig. 2). A total of 74 infarcts (61%) exhibited bubbly consolidation, and 48 lesions (39%) exhibited homogeneous consolidation (Fig. 2). Contrast-enhanced CT images showed that 23 patients had pulmonary vein involvement, 20 of whom had pulmonary congestion (Fig. 3); 30 patients had no pulmonary vein involvement; vein involvement was unable to be determined in 5 patients because of poor visualization of the pulmonary veins, 1 of whom had pulmonary congestion. Pleural effusion was observed in 22 patients (Fig. 2) (Tables 1, 2).

PET Findings

Among the 122 infarcts found in the study, 95 (78%) showed different degrees of increased FDG uptake, which was higher than lung parenchyma, with an SUV_{max} of 1.5 to 6.6 (mean, 3.3 [SD, 1.1]). Forty-two infarcts (34%) manifested as the "rim sign" (elevated FDG uptake along the periphery of pulmonary consolidation), and others (44%) manifested as the "mismatch between PET and CT" (the range of hypermetabolic regions on PET images was smaller than the range of opacities shown on CT images) (Fig. 2). Twenty-seven infarcts (22%) showed no obvious FDG hypermetabolism (Fig. 1). Eight patients (14%) showed a "pleural curvilinear sign" (linear FDG hypermetabolism along the pleura) with an SUV_{max} of 2.4 to 5.0 (mean, 3.4 [SD, 0.8]) (Fig. 4) (Tables 1, 2).

DISCUSSION

The correlation between tumors and pulmonary infarction is controversial. One viewpoint is that tumors are an important cause of pulmonary infarction mainly due to insufficient local perfusion due to tumor oppression or infiltration of the pulmonary artery, blood vessel obstruction by tumor thrombi, or abnormalities in the coagulation system caused by the tumor itself or by antitumor therapy.[11,12] In contrast, some scholars believe that when a tumor oppresses or invades the pulmonary artery, the bronchial artery has sufficient time to establish collateral circulation to supplement insufficient blood perfusion in the corresponding area, and therefore, pulmonary infarction rarely occurs.[13] However, we have found that pulmonary infarction induced by hilar tumors is a common but

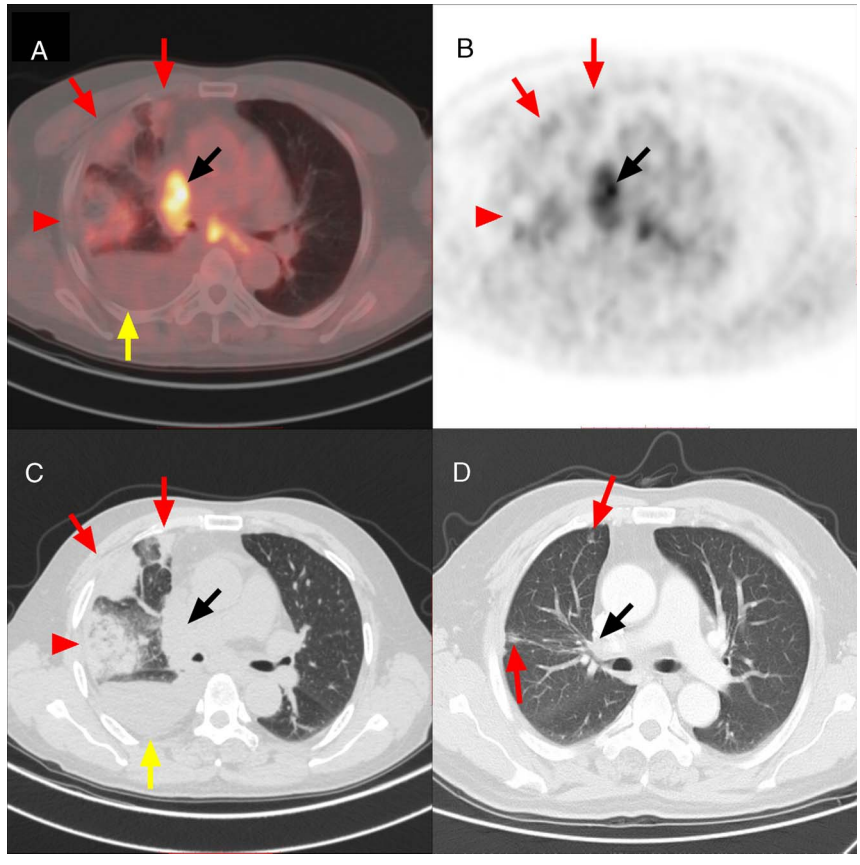

FIGURE 2. A 66-year-old man with small cell lung cancer of the right hilum. Axial PET/CT (**A**), PET (**B**), and chest lung window (**C**) showed an FDG hypermetabolic mass (SUV_{max} = 8.4) in the right hilum (black arrow). Images showed multiple subpleural pulmonary infarcts (red arrow) with homogeneous or bubbly consolidation, which exhibited mild heterogeneous hypermetabolism (SUV_{max} = 3.2, 2.5, and 2.1). The metabolic patterns were "rim sign"(short arrow) or "mismatch between PET and CT"(long arrow). Note the right pleural effusion (yellow arrow). After 2 months of antitumor treatment, axial thin-slice chest CT (**D**) showed the mass in the right hilum was significantly reduced, and the right pulmonary artery was patent (black arrow). Residual fibrous scars were noted in the upper lobe of the right lung (red arrow).

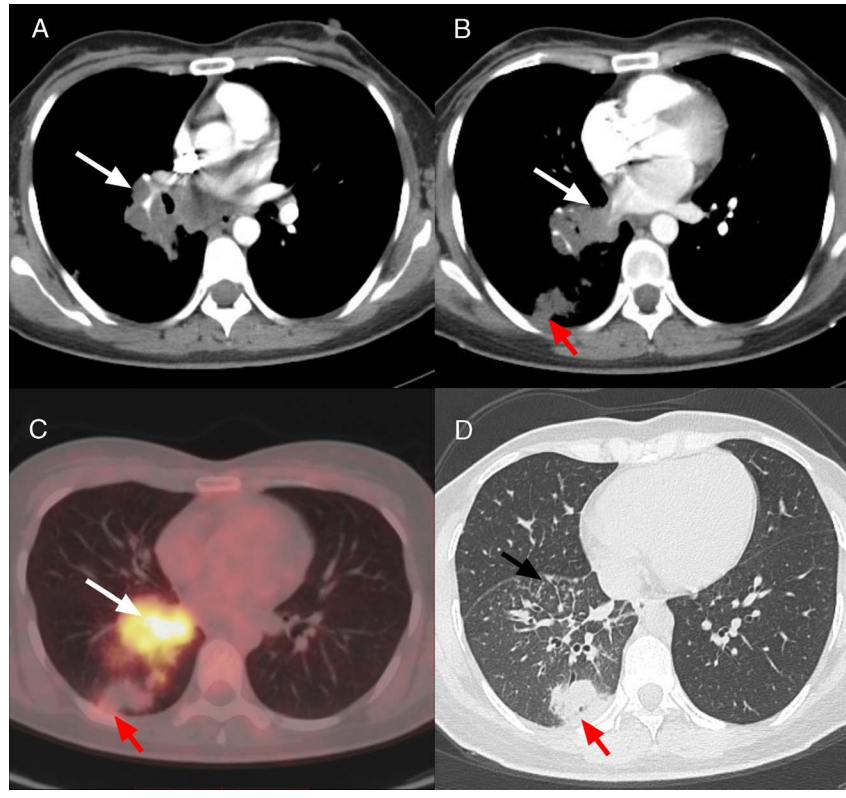

FIGURE 3. A 32-year-old woman with small cell lung cancer of the right hilum. Axial contrast-enhanced CT (**A** and **B**) and PET/CT (**C**) showed an FDG hypermetabolic mass (SUV_{max} = 11.6) in the right hilum (white arrow) with occlusion of the right pulmonary artery and right inferior pulmonary vein. Axial thin-slice chest CT (**D**) showed slight attenuation of the lower lobe of the right lung and thickening of the interlobular septa (black arrow). Images (**B**–**D**) showed a patchy pulmonary infarction in the lower lobe of the right lung (red arrow) with mild heterogeneous hypermetabolism (mismatch between PET and CT).

underrecognized problem. We speculate that this condition is related not only to hilar tumors involving the pulmonary artery but also to the involvement of the other arterial supply system: hilar bronchial arteries. Although the bronchial arteries are thin and difficult to observe, their distribution area is occupied by hilar tumor; thus, we speculate that they are likely to be affected.

In this study, small cell lung cancer was the most common cancer (64%) and was significantly more common than other types of tumors, which might be related to the characteristics of small cell lung cancer. Compared with other types of lung cancer, small cell lung cancer has higher proliferative activity and invasiveness and is more likely to induce hilar masses to invade pulmonary vessels.[14,15] Our study also found that hilar lymph node metastasis in 2 patients with cervical cancer resulted in pulmonary infarction. Marriott and Weisbrod[7] found that metastasis of choriocarcinoma led to hilar tumor–induced pulmonary infarction. Therefore, hilar metastasis of extrapulmonary tumors can also cause pulmonary infarction.

Vascular occlusion can cause changes in hemodynamics and arterial blood gases. When a large pulmonary artery is obstructed, acute dyspnea or syncope may occur simultaneously.[16] In our study, no acute symptoms occurred, perhaps because the relatively slow invasion of the pulmonary arteries by hilar tumors gave the body time to compensate, thereby alleviating clinical symptoms. Among the patients included in our study, the major clinical manifestations were cough (64%) and hemoptysis (36%), whereas chest pain, which is commonly observed in embolic pulmonary infarction, rarely occurred in our study.

This study found that patients with hilar tumor–induced pulmonary infarction mostly had multiple infarcts (62%), which is related to the large range dominated by the large hilar vessels. The 6 cases of giant infarcts in this study also confirmed this speculation. This study did not find a lower lobe predominance for pulmonary infarction as reported in other studies.[3,4,17] Through careful comparison, we found that most previous studies focused on embolic pulmonary infarction and rarely investigated hilar tumor–induced pulmonary infarction. Embolic pulmonary infarction is affected by gravity, and the emboli are more likely to enter the lower lobe with blood flow, while the infarcted location of hilar tumor–induced pulmonary infarction is determined by the pulmonary artery involved by hilar tumors.

Among the 122 infarcts in this study, 58 (48%) manifested as a "Hampton hump." The incidence of this sign was slightly lower than that reported by He et al[17] and Revel et al,[11] perhaps because the overly large size of some infarcts complicated assessments of their morphology. In our study, "bubbly consolidation" was more common (61%) in hilar tumor–induced pulmonary infarction. Regarding the formation mechanism, Balakrishnan et al[18] believed that the central lucencies in the infarct are the residual tissue of the normal pulmonary lobules, and Revel et al[11] believed that the central lucencies tend to represent necrotic pulmonary lobule tissue, whereas the eccentric lucencies tend to represent living pulmonary lobule tissue. We carefully observed the infarcts and found that the lucencies in consolidation areas were usually scattered, and only a few were located in the center, therefore likely representing residual

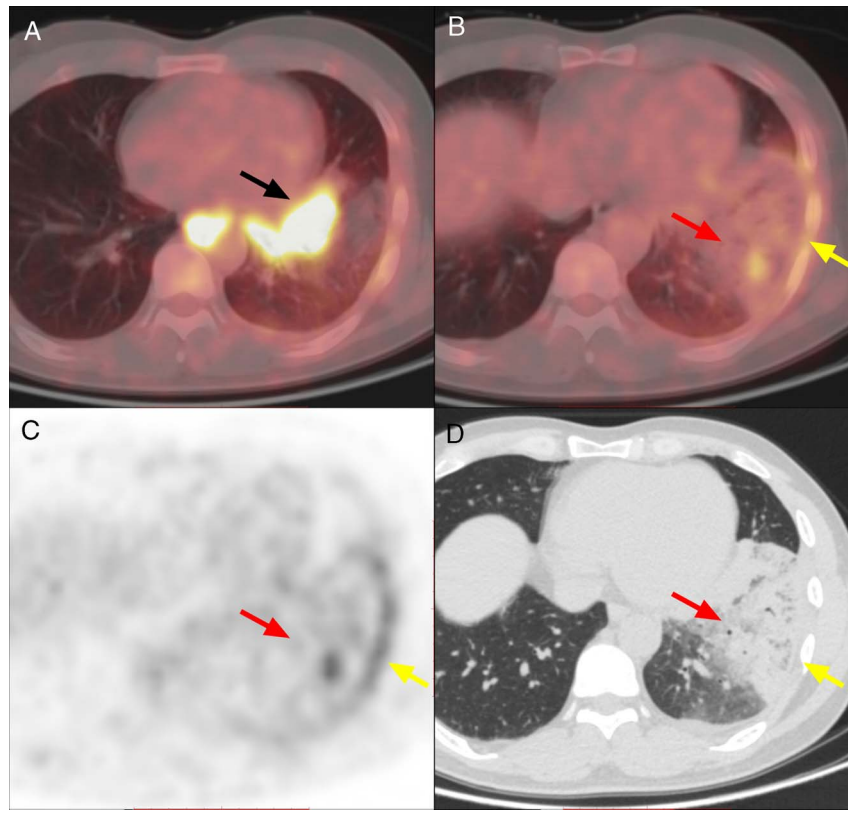

FIGURE 4. A 36-year-old man with lung adenocarcinoma of the right hilum. Axial PET/CT (**A**) showed an FDG hypermetabolic mass (SUV_{max} = 18.8) in the left hilum (black arrow). Axial PET/CT (**B**), PET (**C**), and thin-slice chest CT (**D**) showed a pulmonary infarction in the upper lobe of the left lung with mild heterogeneous hypermetabolism (red arrow) (SUV_{max} = 7.9). Linear FDG hypermetabolism was observed along the left pleura (yellow arrow) (SUV_{max} = 5.0).

normal lung tissue. We believe that this manifestation may be related to the formation mechanism of hilar tumor–induced pulmonary infarction. Compared with acute pulmonary embolism, the process of hilar tumor invasion into hilar vessels is slower, so infarcts are more likely to contain residual lung tissue.

In this study, 23 patients (40%) with pulmonary vein involvement experienced blocked venous return, which is similar to the hemodynamic change in left-sided heart failure, the latter of which is a recognized cause of pulmonary infarction.[1,19,20] Therefore, the formation mechanisms of hilar tumor–induced pulmonary infarction are complex and may be associated with vein involvement. In our study, pleural effusion occurred in 22 patients (38%), and its incidence was higher than that reported by Johnson et al,[21] perhaps because of (1) the increased vascular permeability due to a larger range of pulmonary infarction and greater release of inflammatory factors caused by the hilar tumors and (2) the increased hydrostatic pressure in the capillaries resulting from hilar tumor invasion of pulmonary veins.

In this study, 95 infarcts had elevated and heterogeneous FDG uptake, and 27 infarcts had no FDG uptake. We speculate that this finding was related to the period of infarcts. The increase in FDG uptake in infarcts is related to the inflammatory reaction. The cause of no FDG uptake may be that the pulmonary infarcts are newly formed and still in the stage of congestive hemorrhage, and an inflammatory response has not yet occurred. Infarction in this period can be distinguished from pulmonary inflammatory and malignant lesions on PET images. Many studies have suggested that pulmonary infarction cannot be effectively differentiated from other pulmonary lesions (such as granuloma, inflammation, and tumors) based solely on the SUV because their metabolic values partially overlap.[6,22,23] Hofman and Hicks[24] pointed out that metabolic pattern recognition seems to have considerable value in PET imaging, as it can help us distinguish some lesions with increased FDG uptake and overlapping metabolic intensity. In this study, the metabolic patterns of the "rim sign" and "mismatch between PET and CT" can be well differentiated from nonnecrotic tumors. Hilar tumor–induced pulmonary infarction should also be distinguished from obstructive pneumonia. Obstructive pneumonia mostly manifests as patchy shadows or acinar nodule shadows distributed along the bronchus, without the distribution characteristics of the peripheral zone of the lung. Enhancement can be observed when contrast agents are applied, and no "rim sign" is evident on PET images. Therefore, the combination of metabolic patterns and lesion morphology has high value for the differential diagnosis of pulmonary lesions. Interestingly, among the 58 patients enrolled in our study, 8 patients had a "pleural curvilinear sign," with the SUV_{max} of 2.4 to 5.0 (mean, 3.4 [SD, 0.8]). This phenomenon has not been mentioned in previous studies on pulmonary infarction. We speculate that this finding may be related to the repair response of the affected pleura. In addition, we speculate that another nuclear medicine imaging technology, ventilation/perfusion SPECT, also has potential application value. When hilar tumor–induced pulmonary infarction occurs, the ventilation images may show a ventilation defect matched with the infarcted area and complicated with the noninfarcted area ventilation decreased if pulmonary hilar bronchial stenosis; the perfusion images show a perfusion defect in the innervated area of

pulmonary artery involved by hilar tumor. However, accurate ventilation/perfusion manifestation and its diagnostic value need to be verified by further studies.

Previous studies mostly use imaging findings to diagnose pulmonary infarction. The strength of our investigation was the use of follow-up data to ensure the accuracy of the pulmonary infarction diagnosis in addition to contrast-enhanced CT. Our follow-up was regular based on evaluations of the curative effect in tumor patients, which did not involve additional radiation or economic burdens. To our knowledge, no published studies have proposed the concept of hilar tumor–induced pulmonary infarction, and published data describing the clinical and imaging features are lacking. The results of this investigation will help us more comprehensively understand the FDG PET/CT and clinical manifestations of pulmonary infarction and provide a basis for the standardized management of hilar tumor–induced pulmonary infarction. Our study had several limitations. First, pulmonary infarction diagnosis mainly relied on contrast-enhanced chest CT and imaging follow-ups, which is the lack of histopathological confirmation, the possibility of misdiagnosis remained. Second, the number of valid samples was small, which might have caused some biases in the study results.

CONCLUSION

Malignant tumor cells at the pulmonary hilum can invade adjacent arteries or veins, resulting in pulmonary infarction. The main clinical manifestations were cough and hemoptysis, and chest pain was rare. Multiple infarcts were common, and no lower lobe predominance was noted. When FDG-PET/CT shows a hilar tumor, "Hampton hump," "bubbly consolidation," "rim sign," "pleural curvilinear sign," "mismatch between PET and CT," and "no metabolic consolidation" findings all indicate pulmonary infarction. If necessary, biopsy can be performed to confirm the diagnosis to avoid misdiagnosis and unnecessary antitumor therapy.

REFERENCES

1. Yousem SA. The surgical pathology of pulmonary infarcts: diagnostic confusion with granulomatous disease, vasculitis, and neoplasia. *Mod Pathol*. 2009;22:679–685.
2. Tsao MS, Schraufnagel D, Wang NS. Pathogenesis of pulmonary infarction. *Am J Med*. 1982;72:599–606.
3. Chengsupanimit T, Sundaram B, Lau WB, et al. Clinical characteristics of patients with pulmonary infarction—a retrospective review. *Respir Med*. 2018;139:13–18.
4. Kirchner J, Obermann A, Stückradt S, et al. Lung infarction following pulmonary embolism: a comparative study on clinical conditions and CT findings to identify predisposing factors. *Rofo*. 2015;187:440–444.
5. Ji Y, Shao CC, Cui Y, et al. The diagnostic value of FDG PET/CT and thin-slice high-resolution chest CT in pulmonary intravascular metastasis. *AJR Am J Roentgenol*. 2021;216:769–775.
6. Kamel EM, McKee TA, Calcagni ML, et al. Occult lung infarction may induce false interpretation of ^{18}F-FDG PET in primary staging of pulmonary malignancies. *Eur J Nucl Med Mol Imaging*. 2005;32:641–646.
7. Marriott AE, Weisbrod G. Bronchogenic carcinoma associated with pulmonary infarction. *Radiology*. 1982;145:593–597.
8. Soussan M, Rust E, Pop G, et al. The rim sign: FDG-PET/CT pattern of pulmonary infarction. *Insights Imaging*. 2012;3:629–633.
9. Badr A, Joyce JM, Durick J. Rim of FDG uptake around a pulmonary infarct on PET/CT in a patient with unsuspected pulmonary embolism. *Clin Nucl Med*. 2009;34:285–286.
10. Bray TJP, Mortensen KH, Gopalan D. Multimodality imaging of pulmonary infarction. *Eur J Radiol*. 2014;83:2240–2254.
11. Revel MP, Triki R, Chatellier G, et al. Is it possible to recognize pulmonary infarction on multisection CT images? *Radiology*. 2007;244:875–882.
12. Noble S, Pasi J. Epidemiology and pathophysiology of cancer-associated thrombosis. *Br J Cancer*. 2010;102(Suppl 1):S2–S9.
13. Ishiguro T, Kasahara K, Matsumoto I, et al. Primary pulmonary artery sarcoma detected with a pulmonary infarction. *Intern Med*. 2007;46:601–604.
14. Ballantyne AJ, Clagett OT, Mcdonald JR. Vascular invasion in bronchogenic carcinoma. *Thorax*. 1957;12:294–299.
15. Kalemkerian GP. Small cell lung cancer. *Semin Respir Crit Care Med*. 2016;37:783–796.
16. Terry PB, Buescher PC. Pulmonary infarction: in the beginning: the natural history of pulmonary infarction. *Chest*. 2017;152:1135–1139.
17. He H, Stein MW, Zalta B, et al. Pulmonary infarction: spectrum of findings on multidetector helical CT. *J Thorac Imaging*. 2006;21:1–7.
18. Balakrishnan J, Meziane MA, Siegelman SS, et al. Pulmonary infarction: CT appearance with pathologic correlation. *J Comput Assist Tomogr*. 1989;13:941–945.
19. Dalen JE, Haffajee CI, Alpert JS, et al. Pulmonary embolism, pulmonary hemorrhage and pulmonary infarction. *N Engl J Med*. 1977;296:1431–1435.
20. Schraufnagel DE, Tsao MS, Yao YT, et al. Factors associated with pulmonary infarction. A discriminant analysis study. *Am J Clin Pathol*. 1985;84:15–18.
21. Johnson PT, Wechsler RJ, Salazar AM, et al. Spiral CT of acute pulmonary thromboembolism: evaluation of pleuroparenchymal abnormalities. *J Comput Assist Tomogr*. 1999;23:369–373.
22. George CJ, Tazelaar HD, Swensen SJ, et al. Clinicoradiological features of pulmonary infarctions mimicking lung cancer. *Mayo Clin Proc*. 2004;79:895–898.
23. Bunyaviroch T, Coleman RE. PET evaluation of lung cancer. *J Nucl Med*. 2006;47:451–469.
24. Hofman MS, Hicks RJ. Restaging: should we PERCIST without pattern recognition? *J Nucl Med*. 2010;51:1830–1832.